AMERICAN SOCIETY FOR MICROBIOLOGY | Applied and Environmental Microbiology®

ENZYMOLOGY AND PROTEIN ENGINEERING

# Four Inserts within the Catalytic Domain Confer Extra Stability and Activity to Hyperthermostable Pyrolysin from *Pyrococcus furiosus*

**Xiaowei Gao,[a] Jing Zeng,[a]* Huawei Yi,[a] Fang Zhang,[a] Bing Tang,[a,b] Xiao-Feng Tang[a,b]**

State Key Laboratory of Virology, College of Life Sciences, Wuhan University, Wuhan, China[a]; Hubei Provincial Cooperative Innovation Center of Industrial Fermentation, Wuhan, China[b]

**ABSTRACT** Pyrolysin from the hyperthermophilic archaeon *Pyrococcus furiosus* is the prototype of the pyrolysin family of the subtilisin-like serine protease superfamily (subtilases). It contains four inserts (IS*147*, IS*29*, IS*27*, and IS*8*) of unknown function in the catalytic domain. We performed domain deletions and showed that three inserts are either essential (IS*147* and IS*27*) or important (IS*8*) for efficient maturation of pyrolysin at high temperatures, whereas IS*29* is dispensable. The large insert IS*147* contains Ca3 and Ca4, two calcium-binding Dx[DN]xDG motifs that are conserved in many pyrolysin-like proteases. Mutagenesis revealed that the Ca3 site contributes to enzyme thermostability and the Ca4 site is necessary for pyrolysin to fold into a maturation-competent conformation. Mature insert-deletion variants were characterized and showed that IS*29* and IS*8* contribute to enzyme activity and stability, respectively. In the presence of NaCl, pyrolysin undergoes autocleavage at two sites: one within IS*29* and the other in IS*27*. Disrupting the ion pairs in IS*27* and IS*8* induces autocleavage in the absence of salts. Interestingly, autocleavage products combine noncovalently to form an active, nicked enzyme that is resistant to SDS and urea denaturation. Additionally, a single mutation in IS*29* increases resistance to salt-induced autocleavage and further increases enzyme thermostability. Our results suggest that these extra structural elements play a crucial role in adapting pyrolysin to hyperthermal environments.

**IMPORTANCE** Pyrolysin-like proteases belong to the subtilase superfamily and are characterized by large inserts and long C-terminal extensions; however, the role of the inserts in enzyme function is unclear. Our results demonstrate that four inserts in the catalytic domain of hyperthermostable pyrolysin contribute to the folding, maturation, stability, and activity of the enzyme at high temperatures. The modification of extra structural elements in pyrolysin-like proteases is a promising strategy for modulating global structure stability and enzymatic activity of this class of protease.

**KEYWORDS** hyperthermophilic archaeon, subtilisin, serine protease, insertion sequence, $Ca^{2+}$-binding, thermostability

**Received** 27 November 2016 **Accepted** 17 December 2016

**Accepted manuscript posted online** 21 December 2016

**Citation** Gao X, Zeng J, Yi H, Zhang F, Tang B, Tang X-F. 2017. Four inserts within the catalytic domain confer extra stability and activity to hyperthermostable pyrolysin from *Pyrococcus furiosus*. Appl Environ Microbiol 83:e03228-16. https://doi.org/10.1128/AEM.03228-16.

**Editor** Haruyuki Atomi, Kyoto University



Address correspondence to Bing Tang, tangb@whu.edu.cn, or Xiao-Feng Tang, tangxf@whu.edu.cn.

* Present address: Jing Zeng, Institute of Microbiology, Jiangxi Academy of Sciences, Nanchang, Jiangxi, China.

Hyperthermophiles grow optimally at temperatures greater than or equal to 80°C and are the primary sources of hyperthermostable enzymes (1, 2). The high thermostability of these enzymes make them especially valuable when investigating mechanisms that stabilize protein structure and function at the maximum temperature capable of supporting life. Additionally, they could be used for biocatalysis applications (3). Heterotrophic hyperthermophiles typically use proteins and peptides as their carbon and energy sources; thus, proteases play important metabolic roles in these microorganisms (1, 2). Isolated from geothermally heated marine sediment, *Pyrococcus*

*furiosus* is a heterotrophic archaeon with an optimal growth temperature of 100°C (4). This hyperthermophilic archaeon is highly proteolytic (5–7) and can grow on casein or peptides as the sole carbon source (8). It has been hypothesized that extracellular proteases act as the first step of protein utilization for the growth of *P. furiosus* (9).

Pyrolysin is an extracellular serine protease of *P. furiosus* and characterized as an extremely stable enzyme with a half-life of 4 h at 100°C and maximum activity at 115°C (6). This enzyme is one of the most thermostable proteases known and is prototypical of the pyrolysin family of subtilases. Members of the pyrolysin family are characterized by large inserts and long C-terminal extensions (CTEs) (10). The pyrolysin precursor protein has 1,398 residues, including a 26-residue signal peptide, a 123-residue N-terminal propeptide, a subtilisin-like catalytic domain, and an approximately 740-residue CTE (9, 11). We previously found that the pyrolysin proform (Pls) was converted to a mature form (mPls) at high temperatures through autoprocessing of the N-terminal propeptide and the C-terminal part of the long CTE (approximately 200 residues in length). This autoprocessing suggests that the long CTE consists of a 200-residue C-terminal propeptide and a 540-residue mature CTE (CTEm) that remains attached to the catalytic domain in mPls (12). Both the N- and C-terminal propeptides contribute to the hyperthermostability of pyrolysin, and the CTEm contributes to enzyme stability and activity (12).

The catalytic domain of pyrolysin can be divided into the core (those residues also present in *Bacillus* subtilisins) and inserts (those residues not present in the core) (11). More specifically, the pyrolysin catalytic domain has an unusually large 147-residue insert between the catalytic residues $Asp^{30}$ and $His^{216}$ (IS*147*; $Val^{62}$-$Val^{208}$). In addition, there are three other inserts that include more than six residues, named IS*29* ($Ser^{229}$-$Asn^{257}$), IS*27* ($Pro^{368}$-$Thr^{394}$), and IS*8* ($Asp^{484}$-$Tyr^{491}$). Large inserts can be found in catalytic domains of other hyperthermostable proteases, such as stetterlysin from *Thermococcus stetteri* (11), STABLE protease from *Staphylothermus marinus* (13), and pyrolysin-like proteases predicted in many sequenced genomes of hyperthermophilic archaea. Eukaryotic tripeptidyl peptidase II (TPP II) also has a 200-residue insert located at a position equivalent to IS*147* in the catalytic domain; however, the TPP II insert is not homologous to pyrolysin IS*147*. The TPP II insert is important for the oligomerization of the active enzyme complex (14). In contrast, the roles of the unusually large inserts in hyperthermostable pyrolysin and its homologs in enzyme function are still unknown. We recently identified two high-affinity $Ca^{2+}$-binding sites (Ca1 and Ca2) that are important for enzyme stabilization, but supplementation of $Na^{+}$, $Ca^{2+}$, or $Mg^{2+}$ salts at concentrations similar to those observed in seawater destabilizes pyrolysin, probably due to disturbance of electrostatic interactions on the enzyme surface by metal ions (15). Notably, the frequency of negatively charged residues in the pyrolysin core is doubled compared with that of *Bacillus* subtilisins. The inserts in pyrolysin contain an even higher percentage of negatively charged residues, specifically Asp residues, than those found in the core (11). However, the role of these negatively charged insert residues in the electrostatic interactions necessary for pyrolysin stabilization remains unclear. The purpose of this study was to investigate the functions of the four inserts of pyrolysin using mutational analysis. The results demonstrated that the inserts play important roles in pyrolysin maturation, stability, and activity. Furthermore, modification of IS*29* increased pyrolysin thermostability.

## RESULTS

**The effects of the four inserts within the catalytic domain on pyrolysin maturation.** At high temperatures, Pls converts into mPls through autoprocessing of both the N- and C-terminal propeptides (12). To investigate the roles of IS*147*, IS*29*, IS*27*, and IS*8* in pyrolysin maturation, four insert-deletion variants of Pls, named PlsΔIS*147*, PlsΔIS*29*, PlsΔIS*27*, and PlsΔIS*8*, were constructed (Fig. 1A). Crude proform samples were incubated at 95°C to mature the enzyme. In contrast to Pls that matured efficiently, PlsΔIS*147* and PlsΔIS*27* degraded rather than converting to the mature form (Fig. 1B), suggesting that IS*147* and IS*27* are required for efficient pyrolysin maturation. Similar to

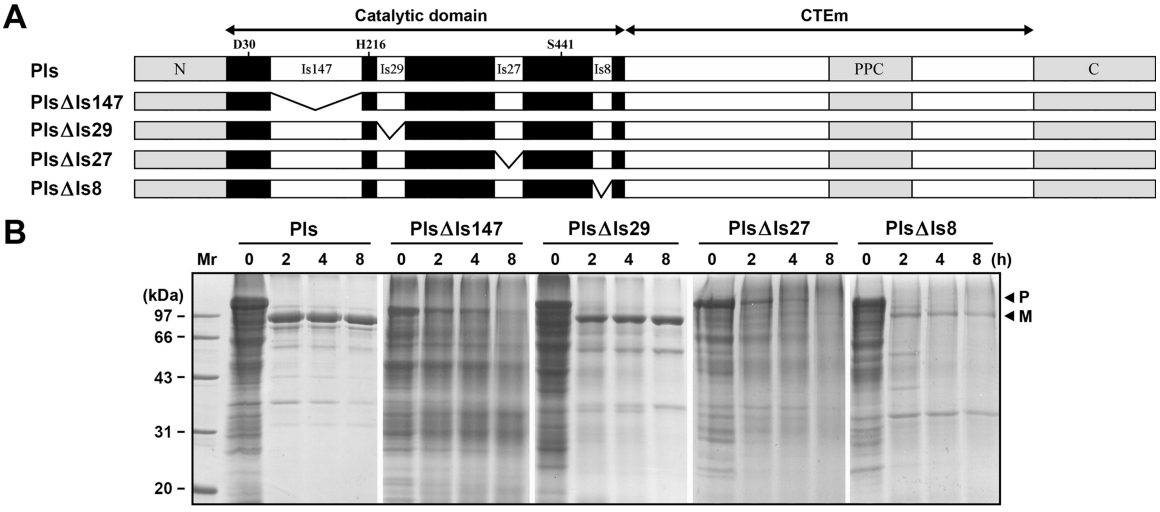


**FIG 1** Maturation of pyrolysin and its variants. (A) A schematic representation of the primary structure of pyrolysin proform (Pls) and its insert-deletion variants. The locations of the active-site residues (Asp[30], His[216], and Ser[441]) and four inserts (IS*147*, IS*29*, IS*27*, and IS*8*) are shown. The core of the catalytic domain is shown in black. The N-terminal propeptide (N), C-terminal extension (CTEm), C-terminal propeptide (C), and putative prepeptidase C-terminal (PPC) domain are indicated. (B) SDS-PAGE analysis of the Pls and variant maturation. Crude samples containing approximately 25 to 30 $\mu$g/ml of Pls and its variants in buffer A were incubated at 95°C for the time intervals indicated and electrophoresed using SDS-PAGE. The positions of the proform (P) and the mature form (M) are indicated on the gels.

Pls, PlsΔIS*29* converted to the mature form efficiently (Fig. 1B), indicating that IS*29* is dispensable for pyrolysin maturation. In the case of PlsΔIS*8*, the variant was able to mature, but the yield of mature protein was much lower than that of Pls (Fig. 1B). Thus, the deletion of IS*8* does not prevent PlsΔIS*8* from folding into a maturation-competent conformation but seems to affect enzyme stability and prevents efficient enzyme maturation at high temperatures.

**IS*147* contains two calcium-binding Dx[DN]xDG motifs important for pyrolysin folding and hyperthermostability.** We previously identified two calcium-binding sites (Ca1 and Ca2) in pyrolysin (15). Sequence analysis of IS*147* revealed two Dx[DN]xDG motifs, Asp[132]-Gly[137] (motif 1) and Asp[161]-Tyr[166] (motif 2) (Fig. 2). The Dx[DN]xDG motif is known to bind calcium, and the side chains of the downstream residues (usually acidic amino acids) can contribute to calcium coordination in the binding site (16, 17). We observed that there are negative-charge-rich DQED and DFTDE sequences located immediately downstream of the two Dx[DN]xDG motifs (Fig. 2). Interestingly, the Ca1 site also contains a DFTDE sequence involved in $Ca^{2+}$ binding (Fig. 2) (15). The Dx[DN]xDG motifs and their downstream sequences are highly conserved in several pyrolysin-like proteases (Fig. 2). We postulated that the two Dx[DN]xDG motifs and their downstream negatively charged residues in pyrolysin are two additional calcium-binding sites (named Ca3 and Ca4).

In the Ca3 site, the conserved Asp[132], Asn[134], and Asp[136] residues of Dx[DN]xDG motif 1 were mutated to Ala to construct single-, double-, and triple-site variants. All variant proforms successfully converted to their mature forms after heat treatment at 95°C (data not shown), implying that these proforms properly fold into the maturation-competent conformation. The purified mature forms of the variants all exhibited specific activity similar to that of wild-type (WT) mPls (Fig. 3A). When incubated at 95°C, the single-site variants (D132A, N134A, and D136A) were more heat resistant than double-site variants (D132A/N134A, N134A/D136A, and D132A/D136A), and the double-site variants were more resistant than the triple-site variant D132A/N134A/D136A (Fig. 3B). These data suggest that Asp[132], Asn[134], and Asp[136] cumulatively contribute to pyrolysin hyperthermostability. While variants D132A, N134A, D136A, and D132N/D136N showed heat inactivation profiles similar to that of the WT at 95°C (Fig. 3B), they retained lower residual activities than that of the WT following incubation with EGTA at 95°C (Fig. 3C). These data indicate that all three mutated residues are involved in calcium binding at the Ca3 site, which is required to stabilize pyrolysin.

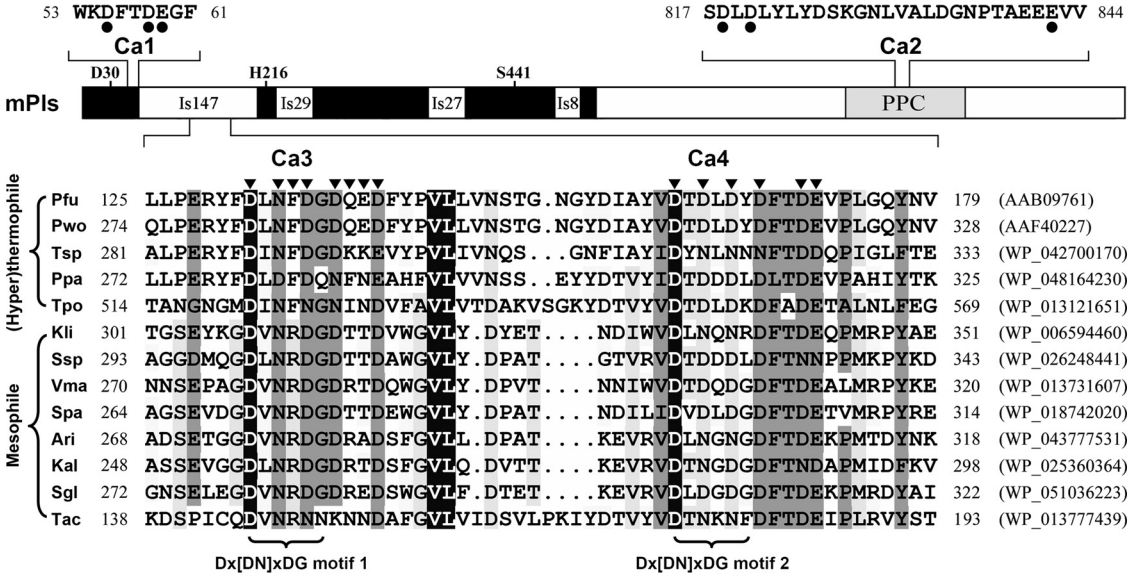


**FIG 2** Alignment of amino acid sequences of pyrolysin and its homologs around two potential $Ca^{2+}$-binding sites (Ca3 and Ca4) within the large insert IS*147*. The target sequence of pyrolysin from *Pyrococcus furiosus* (Pfu) was aligned with that from *Pyrococcus woesei* (Pwo), *Thermococcus* sp. strain PK (Tsp), *Palaeococcus pacificus* (Ppa), *Thermincola potens* (Tpo), *Kineosphaera limosa* (Kli), *Streptomyces* sp. strain LaPpAH-108 (Ssp), *Verrucosispora maris* (Vma), *Salinispora pacifica* (Spa), *Amycolatopsis rifamycinica* (Ari), *Kutzneria albida* (Kal), *Saccharomonospora glauca* (Sgl), and *Tepidanaerobacter acetatoxydans* (Tac). GenBank accession numbers of the proteins are shown in parentheses. The amino acid residues are numbered starting from the N terminus of the precursor or the mature enzyme (Pfu). The two Dx[DN]xDG $Ca^{2+}$-binding motifs are indicated. Arrowheads indicate residues that were mutated. A schematic representation of the primary structure of mature Pls (mPls) and the residues of Ca1 and Ca2 sites (indicated by filled circles) are also shown.

The four residues immediately downstream of Dx[DN]xDG motif 1 ($Asp^{138}$, $Gln^{139}$, $Glu^{140}$, and $Asp^{141}$) (Fig. 2) were simultaneously mutated to Ala. The resulting variant D138A/Q139A/E140A/D141A displayed heat resistance similar to that of the WT under nonchelating conditions (Fig. 3B) but exhibited decreased residual activity compared to

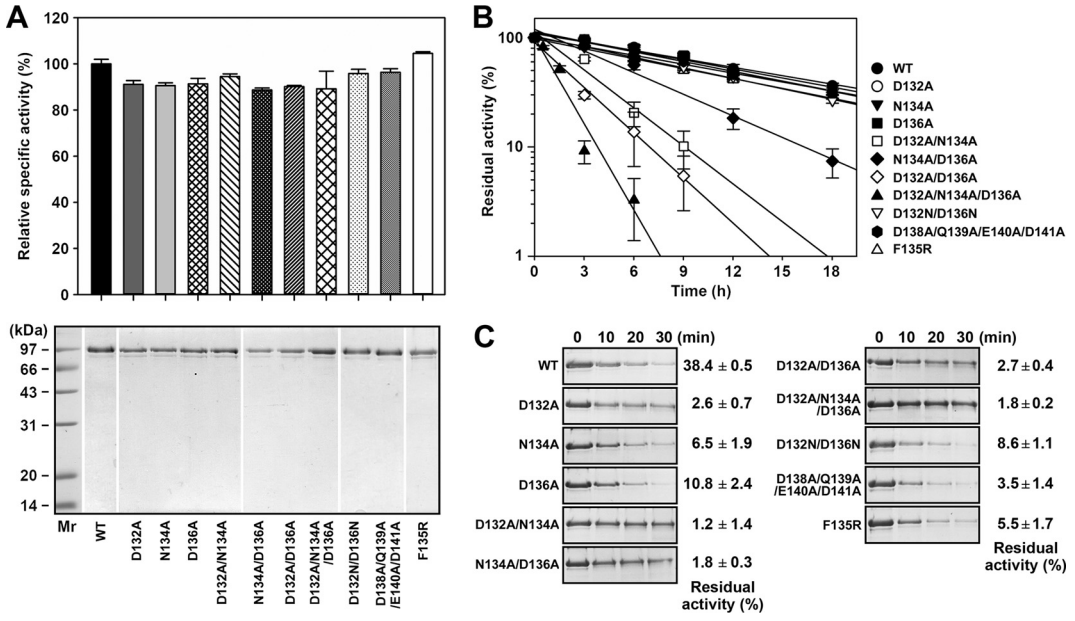


**FIG 3** Mutating residues of the Ca3 site affects pyrolysin activity and stability. (A) SDS-PAGE analysis (lower) and activity assays (upper) of purified samples of mature enzymes. Azocaseinolytic activities of the enzymes were carried out at 95°C in buffer A, and relative activity was calculated by defining the activity of the WT as 100%. (B and C) Heat inactivation profiles. Enzymes (8.0 $\mu$g/ml) in buffer A were incubated at 95°C in the absence (B) or presence (C) of 2 mM EGTA. At the time intervals indicated, samples were removed and an azocaseinolytic activity assay (B and C) and SDS-PAGE (C) were performed. The residual activity is expressed as a percentage of the original activity for each enzyme sample. The values are expressed as means ± standard deviations (SD) from three independent experiments.

the WT following incubation with EGTA at 95°C (Fig. 3C). These results suggest that the residues downstream of motif 1 also contribute to calcium binding at the Ca3 site. Additionally, we noted that the $Phe^{135}$ residue in Dx[DN]xDG motif 1 is conserved in pyrolysin-like proteases from (hyper)thermophiles, whereas the corresponding residue is an Arg in enzymes from mesophiles (Fig. 2A). When the $Phe^{135}$ residue of pyrolysin was mutated to Arg, the thermostability of the resulting variant, F135R, did not change under nonchelating conditions compared to that of the WT (Fig. 3B). However, the F135R variant showed a lower level of residual activity than the WT following incubation with EGTA at 95°C (Fig. 3C). This result implies that a positively charged Arg residue in Dx[DN]xDG motif 1 affects calcium binding at the Ca3 site.

In the presence of EGTA, the protein quantity of very unstable variants (e.g., D132A/N134A, N134A/D136A, and D132A/N134A/D136A) did not decrease as much as that of the WT following heat treatment at 95°C (Fig. 3C). The WT is likely more EGTA resistant than very unstable variants, which made it more susceptible to autodegradation at 95°C. In contrast, the variants did not degrade significantly because the calcium was chelated more easily from their Ca3 sites, leading to a rapid destabilization and inactivation of these variants. This evidence emphasizes the importance of the Ca3 site in maintaining pyrolysin structural stability at high temperatures.

In the Ca4 site, the conserved $Asp^{161}$, $Asp^{163}$, and $Asp^{165}$ residues of Dx[DN]xDG motif 2, as well as the downstream residues $Asp^{167}$, $Asp^{170}$, and $Glu^{171}$, were mutated to Ala. Crude proform samples were incubated at 95°C to undergo enzyme maturation; however, none of the Ca4 site variants matured as efficiently as the WT (Fig. 4A), indicating that the Ca4 site is important for pyrolysin maturation. During the incubation period, the concentrations of the D161A, D161A/D165A, D161A/D163A/D165A, and D167A/D170A/E171A variant proforms decreased gradually. However, minimal mature enzyme was detected (Fig. 4A), and the samples showed no detectable proteolytic activity (data not shown). These data suggest that the four variants are maturation defective. Proteins are known to suffer from thermogenic hydrolysis at high temperatures, and the susceptibility of a protein to thermogenic hydrolysis depends on the conformational integrity of the protein at that temperature (18). It is possible that the maturation-defective proforms are less resistant to thermogenic hydrolysis than the WT, leading to degradation rather than maturation at 95°C. To test this hypothesis, proforms of WT and D161A/D163A/D165A were constructed with an S441A active-site mutation and purified (Fig. 4B). The D161A/D163A/D165A/S441A proform degraded more than the S441A proform at 95°C (Fig. 4C), confirming that the replacement of $Asp^{161}$, $Asp^{163}$, and $Asp^{165}$ with Ala affects structural stability of the proform and makes it more susceptible to thermogenic hydrolysis. The D163A, D165A, D161A/D163A, D163A/D165A, and D161N/D163N/D165N variant proforms were capable of maturation, but the yields of mature enzymes were very low (Fig. 4A). Compared with the WT, the purified mature forms of D163A and D161N/D163N/D165N (Fig. 4B) had similar heat inactivation profiles at 95°C, either in the absence or presence of EGTA (Fig. 4D), and exhibited similar (D161N/D163N/D165N) or slightly lower (D163A) activity levels (Fig. 4E). We showed previously that only correctly folded proforms of pyrolysin matured efficiently and that the proform is less stable than the mature form with respect to thermogenic hydrolysis resistance (12). Given this information, the low maturation efficiencies of the Ca4 site variants (e.g., D163A and D161N/D163N/D165N) could be due to slower folding and lower maturation rates compared to those of the WT. It is likely that a small amount of the proform variants was converted to the stable mature form, and most of the proform was degraded by thermogenic hydrolysis or proteolysis by the mature enzyme. Taking these findings together, the Ca4 site plays an important role in the folding of pyrolysin into a maturation-competent conformation at high temperatures.

The calcium ion contents of pyrolysin and its Ca3 and Ca4 site variants were determined. To prevent autocleavage of the enzymes during sample preparation, the active-site variant S441A and its Ca3 and Ca4 site variants (D132A/N134A/D136A/S441A and D161N/D163N/D165N/S441A) were purified (Fig. 4B) and used for inductively

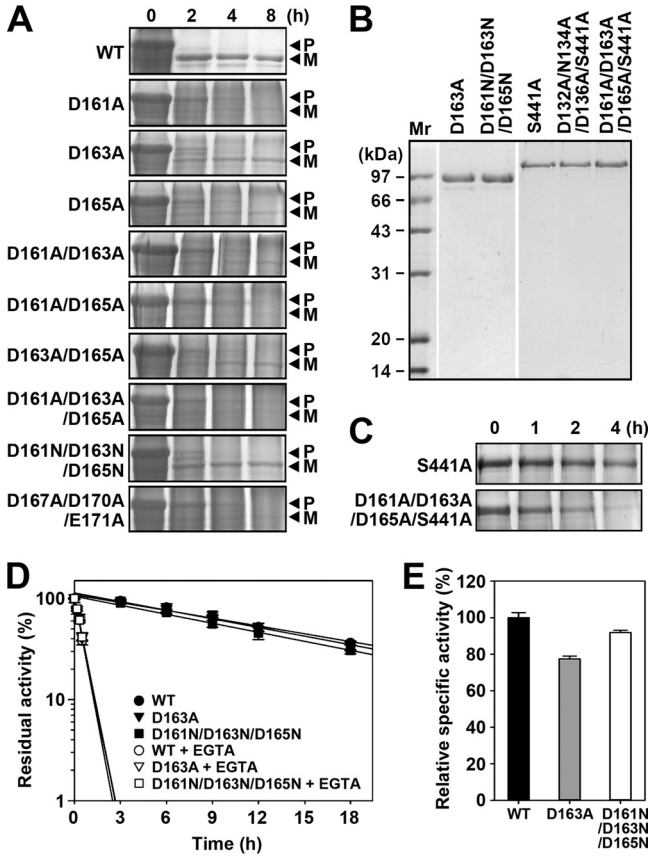


**FIG 4** Properties of pyrolysin Ca4 site variants. (A) SDS-PAGE analysis of variant maturation. Crude samples of the variants in buffer A were incubated at 95°C for the time intervals indicated and electrophoresed using SDS-PAGE. The positions of the proform (P) and the mature form (M) are indicated on the gels. (B) SDS-PAGE analysis of purified samples of the variants. (C) Thermogenic hydrolysis of active-site variants. Purified samples of the variant proforms (8.0 $\mu$g/ml) in buffer A were incubated at 95°C for the time intervals indicated and electrophoresed using SDS-PAGE. (D) Heat inactivation profiles. The enzymes (8.0 $\mu$g/ml) in buffer A were incubated at 95°C in the absence or presence of 2 mM EGTA for the time intervals indicated, and activity was tested using the azocaseinolytic activity assay. The residual activity is expressed as a percentage of the original activity of each enzyme sample. (E) Activity assay of purified mature enzymes. Azocaseinolytic activities of the enzymes were determined at 95°C in buffer A, and relative activity was calculated by defining the activity of the WT as 100%. (D and E) The values are expressed as means ± SD from three independent experiments.

coupled plasma mass spectrometry (ICP-MS) analysis. As shown in Table 1, S441A bound at least four calcium ions, while D132A/N134A/D136A/S441A and D161N/D163N/D165N/S441A contained approximately three and two calcium ions, respectively. These data confirm that the Ca3 and Ca4 sites of pyrolysin are involved in calcium binding. We noticed that D161N/D163N/D165N/S441A contained fewer calcium ions than D132A/N134A/D136A/S441A (Table 1). One reasonable explanation for this is that the disruption of the Ca4 site, which is critical for pyrolysin folding, may prevent other binding sites from adopting a proper conformation to bind calcium ion.

**TABLE 1** Calcium ion content of S441A and its Ca3 and Ca4 site variants, as determined by ICP-MS[a]

| Enzyme | Amt of $Ca^{2+}$/molecule (mol/mol) |
|---|---|
| S441A | 4.38 ± 0.20 |
| D132A/N134A/D136A/S441A | 3.13 ± 0.25 |
| D161A/D163A/D165A/S441A | 2.07 ± 0.08 |

[a]Calcium ion concentration in the dialysis buffer was subtracted from the concentrations in the corresponding protein samples prior to calculating the calcium ion content per enzyme molecule. Values are expressed as means ± SD from two independent experiments.

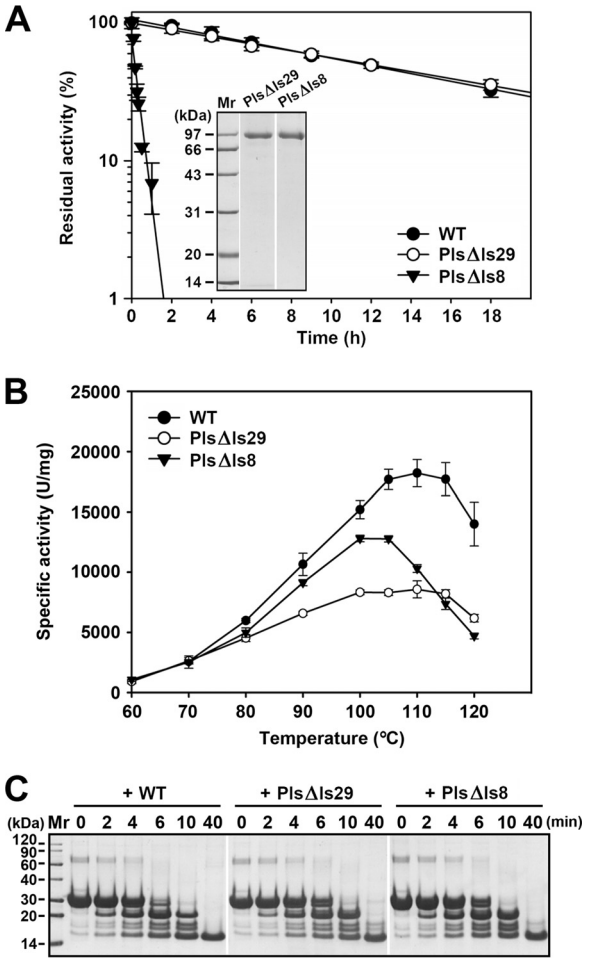


**FIG 5** Properties of mature PlsΔIS*29* and PlsΔIS*8*. (A) Heat inactivation profiles. The enzymes (8.0 $\mu$g/ml) were incubated at 95°C in buffer A for the time intervals indicated, and an azocaseinolytic activity assay was performed. Residual activity is expressed as a percentage of the original activity of each enzyme sample. The inset shows the SDS-PAGE analysis of purified mature PlsΔIS*29* and PlsΔIS*8*. (B) Temperature dependence of azocaseinolytic activity. Activity assays were performed in buffer A for 10 min at the indicated temperatures using 0.5% azocasein as the substrate. The values are expressed as means ± SD (bars) from three independent experiments. (C) Digestion patterns of $\beta$-casein cleaved by the enzymes. The reaction was carried out at 85°C in buffer A containing 0.1 mg/ml of $\beta$-casein and 0.5 nM enzyme for different time periods, and then the samples were subjected to tricine-SDS-PAGE analysis.

**IS*29* and IS*8* confer additional activity and stability to pyrolysin at high temperatures.** Compared with the WT, mature PlsΔIS*29* showed no significant change in stability at 95°C (Fig. 5A) but exhibited lower azocaseinolytic activity at temperatures of 80 to 120°C (Fig. 5B). This result indicates that insert IS*29* plays a role in improving enzymatic activity rather than contributing to stability at high temperatures. Additionally, mature PlsΔIS*29* had lower $K_m$ and $k_{cat}$ values for the synthetic substrate suc-AAPK-pNA than the WT at 90°C (Table 2). This result suggests that deletion of IS*29* increases substrate affinity and decreases the turnover rate of the enzyme. Unlike mature

**TABLE 2** Kinetic parameters of mature forms of WT pyrolysin and its variants[a]

| Enzyme | $K_m$ (mM) | $k_{cat}$ ($s^{-1}$) |
|---|---|---|
| WT | 2.27 ± 0.32 | 1,726 ± 71 |
| PlsΔIS*29* | 1.27 ± 0.15 | 617 ± 59 |
| PlsΔIS*8* | 2.50 ± 0.11 | 1,608 ± 53 |

[a]The kinetic parameters were determined at 90°C using suc-AAPK-pNA as the substrate (described in Materials and Methods). Values are expressed as means ± SD from three independent experiments.

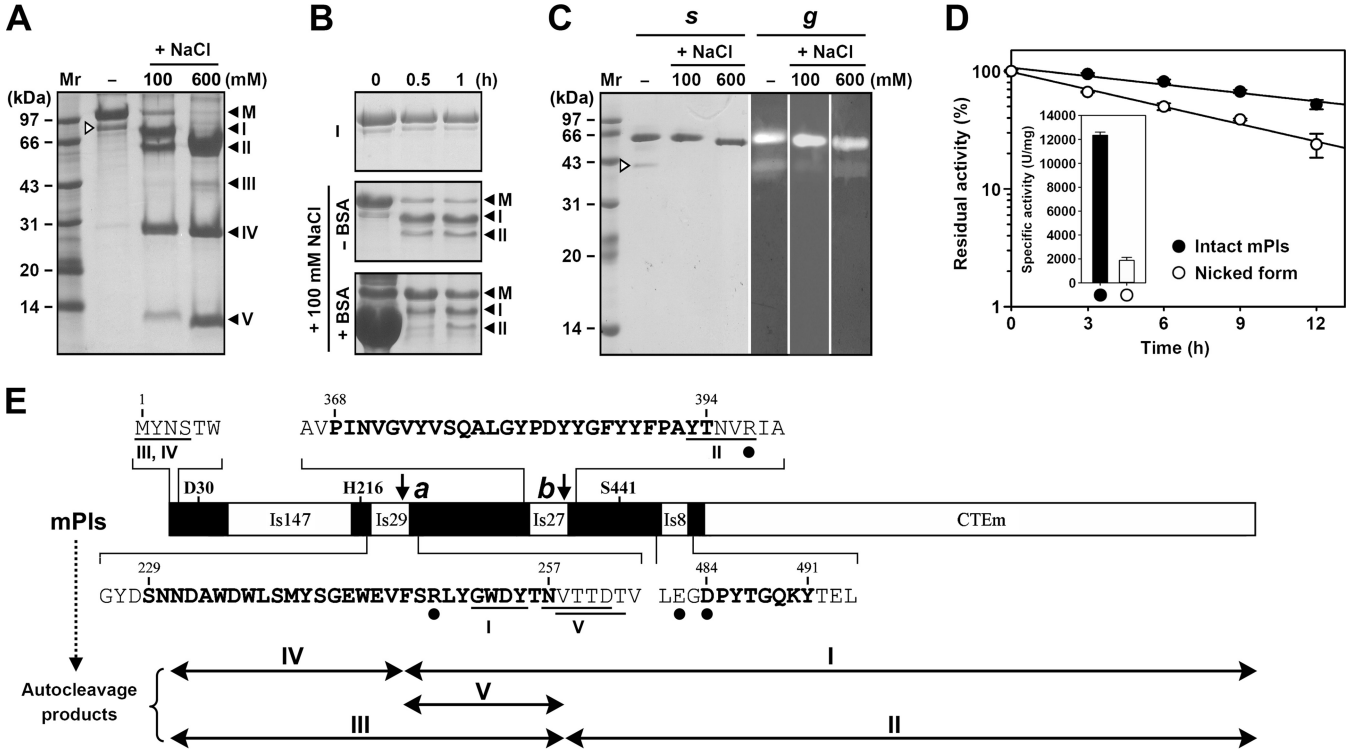


**FIG 6** Salt-induced formation of nicked pyrolysin. (A) SDS-PAGE analysis of mPls salt-induced autocleavage. The purified sample (15.0 $\mu$g/ml) of mPls in buffer A was incubated at 95°C for 1 h in the absence (−) or presence (+) of 100 or 600 mM NaCl. The proteins were precipitated with TCA and electrophoresed using tricine–SDS-PAGE. Samples incubated in 100 or 600 mM NaCl were loaded with a 4-fold increase in protein concentration compared with samples without NaCl. The positions of mPls (M) and the autocleavage products (I, II, III, IV, and V) are indicated with closed arrowheads, and Md is indicated with an open arrowhead. Bands of products I to V were assessed using N-terminal sequencing. (B) Effects of BSA on pyrolysin autocleavage. A purified sample (15.0 $\mu$g/ml) of mPls in buffer A with (+) or without (−) 100 mM NaCl was incubated at 95°C in the absence (−) or presence (+) of BSA (150.0 $\mu$g/ml). At the time intervals indicated, aliquots were withdrawn, precipitated with TCA, and analyzed using tricine–SDS-PAGE. The positions of mPls (M) and the autocleavage products I and II are indicated with closed arrowheads. (C) Urea–SDS-PAGE and gelatin overlay assays of nicked pyrolysin. Enzyme samples were electrophoresed using urea–SDS-PAGE (*s*), and a gelatin overlay assay was performed at 90°C (*g*). (D) Stability and activity of nicked enzyme. The enzymes (8.0 $\mu$g/ml) were incubated at 95°C in buffer A for the time intervals indicated and analyzed using an azocaseinolytic activity assay. Residual activity is expressed as a percentage of the original activity of each enzyme. The inset shows the specific activities of the enzymes against azocasein (0.5%) at 95°C. (E) Schematic representation of the primary structure of mPls and the identified autocleavage sites. The amino acid sequences of inserts IS*29*, IS*27*, and IS*8* are indicated in boldface. The first four or five residues of products I to V, identified by N-terminal sequencing, are underlined. The locations of the two autocleavage sites *a* and *b* (Tyr$^{251}$-Gly$^{252}$ and Ala$^{392}$-Tyr$^{393}$ bonds) are indicated with vertical arrows. Double-headed arrows show the salt-induced autocleavage products of mPls. Residues predicted to be involved in ionic interactions and subsequently mutated are indicated with filled circles.

PlsΔIS*29*, the thermostability of mature PlsΔIS*8* dramatically decreased at 95°C (Fig. 5A), indicating that IS*8* plays an important role in stabilizing pyrolysin structure. Compared with the WT, mature PlsΔIS*8* had reduced azocaseinolytic activity at temperatures above 80°C and a concomitant downshift in optimum activity temperature (Fig. 5B). The $K_m$ and $k_{cat}$ values of PlsΔIS*8* at 90°C were similar to those of the WT (Table 2), implying that deletion of IS*8* does not affect the catalytic behavior of pyrolysin. The decreased activity of mature PlsΔIS*8* above 80°C is most likely due to destabilization of the variant at high temperatures. The digestion pattern of $\beta$-casein cleaved by PlsΔIS*29* or PlsΔIS*8* was essentially the same as that by the WT (Fig. 5C), suggesting that IS*29* and IS*8* do not contribute significantly to the cleavage specificity of pyrolysin.

**Salt-induced autocleavage within IS*29* and IS*27* produces nicked pyrolysin.** We showed previously that pyrolysin undergoes autocleavage when supplemented with various salts (15). Here, the cleavage sites were identified by N-terminal sequencing. Following 100 mM NaCl incubation at 95°C for 1 h, mPls was cleaved into five products, named I, II, III, IV, and V (Fig. 6A). N-terminal sequencing of the five products revealed that cleavage at the Tyr$^{251}$-Gly$^{252}$ bond (site *a*) within IS*29* produced products I and IV, and cleavage at the Ala$^{392}$-Tyr$^{393}$ bond (site *b*) within IS*27* produced products II and III (Fig. 6E). Product V contained two polypeptides. The first five amino acid residues were NVTDD and VTTDT and were located five and six residues downstream of site *a*,

respectively (Fig. 6E). When the NaCl concentration was increased to 600 mM, the level of product I decreased and the levels of the products II and V increased (Fig. 6A). These data suggest that the latter two products could be generated by cleavage of product I at site *b*. The product III level was much lower than those of the other four products (Fig. 6A), implying that product III can be converted to other products, such as IV and V. Autocleavage of mPls at both the *a* and *b* sites generates an intersite fragment that undergoes an N-terminal truncation of five or six residues to yield product V. When incubated with NaCl in the presence of bovine serum albumin (BSA) (Fig. 6B), mPls degradation was reduced compared with incubation without BSA, suggesting that the addition of BSA decreases proteolysis of the enzyme via intermolecular interactions. In addition, purified mPls contained a small amount of an 80-kDa contaminant named Md (Fig. 6A). Md was previously identified as an mPls degradation product produced by C-terminal truncation (15). Md exhibited proteolytic activity in the absence of trichloroacetic acid (TCA) treatment and was degraded and inactivated in the presence of salt (Fig. 6C).

Interestingly, while TCA treatment followed by SDS-PAGE analysis showed five cleaved products (Fig. 6A), the same samples without TCA treatment showed a single band with an apparent molecular mass similar to that of the intact mPls subjected to SDS-PAGE with 8 M urea (Fig. 6C). The single band exhibited proteolytic activity based on a gelatin overlay assay performed at 90°C (Fig. 6C). These results show that the five autocleavage products can form a stable, active nicked enzyme that is resistant to SDS and urea denaturation. The nicked enzyme generated at 600 mM NaCl (Fig. 6A and C) was dialyzed to remove the salt. The half-life of the nicked enzyme was shorter than that of the intact mPls at 95°C (Fig. 6D), suggesting that autocleavage at sites *a* and *b* affects pyrolysin thermostability. Additionally, the nicked enzyme had reduced azocaseinolytic activity compared with intact mPls (Fig. 6D). As mentioned above, IS*29* is important for the enzymatic activity of pyrolysin. The cleavage of the $Tyr^{251}$-$Gly^{252}$ bond (site *a*) in IS*29* could be related to the decreased activity of the nicked enzyme.

**The insert-mediated electrostatic interactions contribute to pyrolysin's resistance to autocleavage.** Once we determined that salt-induced autocleavage of mPls occurs within IS*29* and IS*27*, we hypothesized that the inserts contribute to structural integrity through electrostatic interactions and that the addition of salts destabilizes the enzyme by disturbing those electrostatic interactions. A previous homology modeling study of the catalytic domain core of pyrolysin (11) predicted that the $Arg^{397}$ and $Glu^{482}$ residues form an ion pair. The $Arg^{397}$ and $Glu^{482}$ residues are located near the C and N termini of IS*27* and IS*8*, respectively (Fig. 6E). We further postulated that the negatively charged $Asp^{484}$ residue residing in IS*8* (Fig. 6E) could interact with $Arg^{397}$. Therefore, $Arg^{397}$, $Glu^{482}$, and $Asp^{484}$ were mutated to probe their roles in enzyme stability.

Compared with the WT, mature forms of the variants R397A, R397E, D484A, and D484N had higher levels of autocleavage during the incubation at 95°C in the absence of additional NaCl. They were cleaved into products II and III (Fig. 7A), and the residual activity decreased remarkably following heat treatment at 95°C for 12 h (Fig. 7B). This indicates that $Arg^{397}$ and $Asp^{484}$ play important roles in enzyme stability. SDS-PAGE analysis revealed that product II of variants R397A, R397E, D484A, and D484N contained two bands with similar but not identical molecular weights (Fig. 7A). The slightly smaller one corresponded to product II generated from mPls in the presence of NaCl (data not shown). This result implies that mutation of $Arg^{397}$ and $Asp^{484}$ leads to cleavage at both site *b* ($Ala^{392}$-$Tyr^{393}$ bond) and a site located a few residues upstream of $Ala^{392}$ (Fig. 6E). Variants E482A and E482Q could also be converted into products II and III, albeit to a lesser extent (Fig. 7A). These variants had reduced residual activity compared with the WT following heat treatment at 95°C for 12 h (Fig. 7B), suggesting that $Glu^{482}$ also contributes to enzyme stability. Compared with the single-site variants E482Q and D484N, the double-site variant E482Q/D484N had increased autocleavage (Fig. 7A) and reduced heat resistance (Fig. 7B). These data indicate that $Glu^{482}$ and $Asp^{484}$ act cumulatively to stabilize the enzyme. Taken together, these results demonstrate that

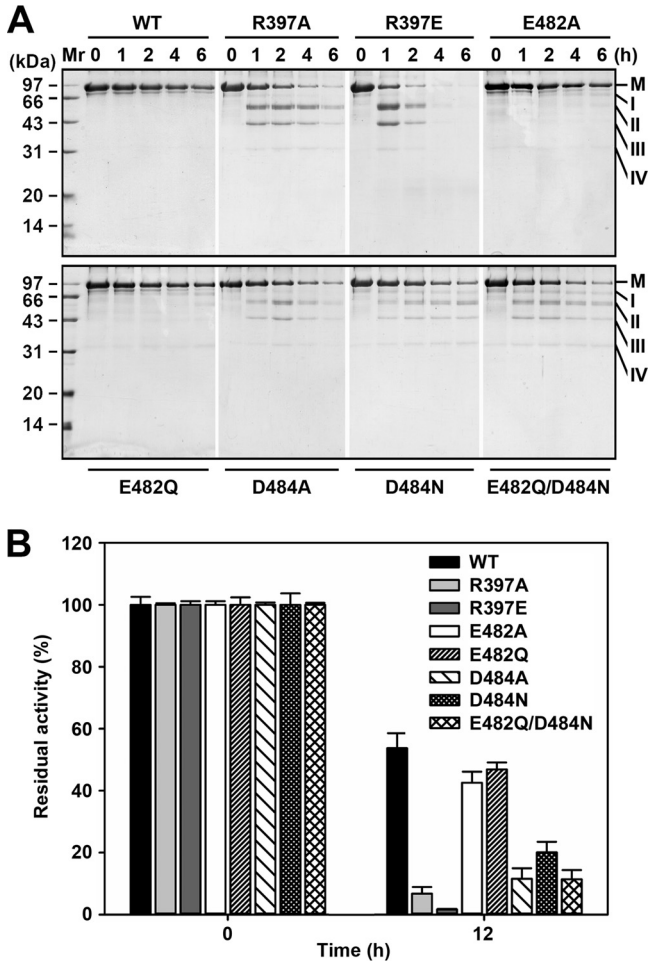


**FIG 7** Mutation of residues involved in ionic interactions affects pyrolysin stability. (A) SDS-PAGE analysis of variant autocleavage. Purified samples (8.0 $\mu$g/ml) of mPIs (WT) and its variants in buffer A were incubated at 95°C for the time intervals indicated and analyzed using SDS-PAGE. The positions of the mature form (M) and autocleavage products (I, II, III, and IV) are indicated. (B) Thermostabilities of the variants. The purified samples (8.0 $\mu$g/ml) of the WT and its variants in buffer A were incubated at 95°C for 12 h and analyzed using an azocaseinolytic activity assay. Residual activity is expressed as a percentage of the original activity of each enzyme sample. The values are expressed as means ± SD (bars) from three independent experiments.

disruption of the putative ion pair(s) involving $Arg^{397}$, $Glu^{482}$, and $Asp^{484}$ makes site *b* in IS*27* more sensitive to proteolysis, which destabilizes the enzyme. In addition, minor products I and IV were detected during incubation of the aforementioned variants (Fig. 7A). The mutations of $Arg^{397}$, $Glu^{482}$, and $Asp^{484}$ appear to enhance the sensitivity of site *a* to proteolysis, likely due to structural changes induced by disruption of the ion pairs or the cleavage at site *b*.

**Modification of IS*29* improves the thermostability of pyrolysin.** In IS*29*, there is a positively charged $Arg^{249}$ residue near autocleavage site *a* (Fig. 6E). To investigate whether $Arg^{249}$ is involved in electrostatic interactions important for enzyme stability, we replaced it with a negatively charged Glu (variant R249E). The purified mature form of R249E (Fig. 8A) was incubated at 95°C in the absence of supplemental NaCl, and none of the autocleavage products were detected (data not shown). Moreover, R249E was more thermostable than the WT (Fig. 8A). R249E also resisted autocleavage better than the WT at 95°C, even in the presence of 100 mM NaCl (Fig. 8B). These results suggest that $Arg^{249}$ does not form a favorable electrostatic interaction to stabilize the enzyme. Instead, $Arg^{249}$ appears to form unfavorable electrostatic interactions that destabilize pyrolysin.

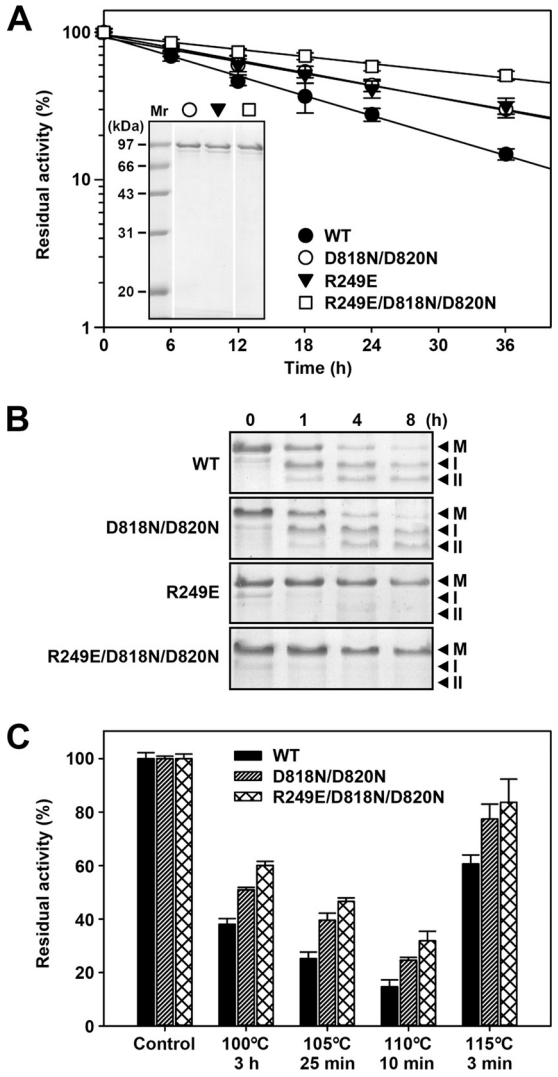


**FIG 8** Mutation of Arg$^{249}$ in IS*29* affects pyrolysin stability. (A and C) Heat inactivation of enzymes. Enzyme samples (8.0 $\mu$g/ml) in buffer A were incubated at 95°C (A) or 100 to 115°C (C) for the time intervals indicated and analyzed using an azocaseinolytic activity assay. Residual activity is expressed as a percentage of the original activity of each enzyme sample (control). The values are expressed as means ± SD (bars) from three independent experiments. The inset shows SDS-PAGE analysis of purified mature proteins. (B) SDS-PAGE analysis of the salt-induced autocleavage of the enzymes. The enzymes (8.0 $\mu$g/ml) in buffer A containing 100 mM NaCl were incubated at 95°C for the time intervals indicated and electrophoresed using SDS-PAGE. The positions of the mature form (M) and autocleavage products I and II are indicated with closed arrowheads.

Our previous study showed that Asn substitutions at the Ca2 site residues Asp$^{818}$ and Asp$^{820}$ in pyrolysin enhances the thermostability of the enzyme (15). When incubated at 95°C, the variants R249E and D818N/D820N had a similar half-life of approximately 18 h, which is longer than that of the WT (approximately 12 h) (Fig. 8A). However, R249E was more resistant to salt-induced autocleavage than D818N/D820N (Fig. 8B). When we combined the mutations to make the variant R249E/D818N/D820N, we increased both half-life at 95°C (approximately 36 h) (Fig. 8A) and salt-induced autocleavage resistance (Fig. 8B). Furthermore, R249E/D818N/D820N retained higher activity levels after heat treatment at 100 to 115°C than the variant D818N/D820N (Fig. 8C).

## DISCUSSION

In this study, the deletion of IS*147* impeded pyrolysin maturation, indicating that this unusually large insert is indispensable for folding the enzyme into a maturation-

competent conformation at high temperatures. IS*147* contained two calcium-binding sites (Ca3 and Ca4), each containing a Dx[DN]xDG motif and at least three downstream negatively charged residues. The Ca4 site does not contribute to pyrolysin stability and activity; however, it is crucial for proper folding and efficient maturation of the enzyme. Other subtilases, such as Tk-subtilisin from *Thermococcus kodakaraensis* (19) and PfSUB1 from *Plasmodium falciparum* (20, 21), require a Dx[DN]xDG-containing insert to fold properly. In Tk-subtilisin, a 20-residue insert containing a Dx[DN]xDG motif is located between the catalytic $His^{153}$ and $Ser^{324}$ residues and is involved in calcium binding (22). Calcium binding by this insert helps the protein fold into the central $\alpha\beta\alpha$-substructure, which is crucial for bacterial subtilisin folding (19, 23). Although IS*147* differs in length and catalytic domain location from the 20-residue insert of Tk-subtilisin, it may enhance pyrolysin folding in a similar manner. Specifically, calcium binding to Dx[DN]xDG motif 2 (Ca4 site) allows IS*147* to adopt the correct structure, facilitating the proper orientation of structure elements in the catalytic domain core. In addition, we found that the Ca3 site contributes to pyrolysin hyperthermostability. Calcium binding to Dx[DN]xDG motif 1 could improve the stability of the IS*147* structure, which in turn contributes to proper catalytic core folding at high temperatures.

The dual Dx[DN]xDG motifs in pyrolysin IS*147* are conserved in many pyrolysin-like proteases (Fig. 2). We found that replacement of $Phe^{135}$ with Arg in Dx[DN]xDG motif 1 affects calcium binding at the Ca3 site of pyrolysin, leading to decreased enzyme stability under chelating conditions. Notably, the Phe residue is conserved in the Dx[DN]xDG motif 1 of pyrolysin-like proteases from (hyper)thermophiles, whereas the Arg residue is conserved in those from mesophiles (Fig. 2). In this context, increasing the calcium affinity of Dx[DN]xDG motif 1 is an important adaptation for pyrolysin-like proteases to function at high temperatures.

Eukaryotic TPP II and STABLE protease from *Staphylothermus marinus* contain large, approximately 200-residue inserts located between catalytic Asp and His residues (named the DH insert); however, these inserts are not homologous to pyrolysin IS*147*. The DH insert of human TPP II is needed for oligomerization, which is critical for fully activating TPP II (14). A structured protrusion within the DH insert (named domain C) is located at the dimer interface of human TPP II and undergoes structural changes upon enzyme complex assembly (24, 25). However, domain C is not present in pyrolysin IS*147* (25). While the DH inserts of human TPP II and STABLE protease lack sequence homology with IS*147*, they contain a Dx[DN]xDG motif (13, 14) corresponding to Dx[DN]xDG motif 2 in IS*147*. Based on the finding that Dx[DN]xDG motif 2 is critical for pyrolysin folding, we hypothesize that the Dx[DN]xDG motifs in the human TPP II and STABLE protease DH inserts contribute to proper enzyme folding.

IS*29* is located in a surface loop adjacent to the C terminus of an $\alpha$-helix that contains the catalytic $His^{216}$ residue (11). *Bacillus* subtilisins (26), thermitase (27), and Tk-subtilisin (22) lack an insert corresponding to IS*29* but have a surface loop containing a conserved high-affinity calcium-binding site (site A) at the same position. Site A plays an important role in subtilisin stabilization (28). In addition, a stabilizing substitution (I79A) located at the C terminus of the $\alpha$-helix containing the catalytic $His^{71}$ residue in subtilisin-like WF146 protease enhances enzymatic activity, probably due to stabilization of the $His^{71}$-containing $\alpha$-helix, which orients the catalytic triad (Asp-His-Ser) into a favorable conformation (29). Interestingly, PlsΔIS*29* showed a decreased activity and had lower $K_m$ and $k_{cat}$ values than the WT. Additionally, PlsΔIS*29* also has a lower binding capacity for bacitracin-Sepharose 4B resin during purification than other mature forms of pyrolysin (data not shown). These data reinforce the hypothesis that deleting IS*29* causes a structural change in the substrate-binding site. Therefore, IS*29* may influence the orientation of the neighboring $\alpha$-helix that contains the catalytic $His^{216}$ residue and enhance pyrolysin activity.

IS*27* is also located in a surface loop (11) and is essential for pyrolysin maturation. Compared with the catalytic domain core and the other three inserts studied here, IS*27* contains a much higher percentage of hydrophobic residues (48%) as well as three Pro residues that can restrict conformational freedom of the polypeptide backbone. The

solvent-exposed IS*27* is theorized to adopt a compact and stable structure that contributes to protein hyperthermostability and is required for proper pyrolysin folding and maturation at high temperatures. The formation of a compact structure by IS*27* also may facilitate the proper orientation of structure elements in the catalytic domain core in a manner similar to that of IS*147*.

While IS*8* is not essential for pyrolysin folding or maturation, it plays a crucial role in stabilization. The stabilizing effect of IS*8* on pyrolysin is closely related to its involvement in electrostatic interactions important for structural integrity of the enzyme. Our previous study demonstrated that the CTE of pyrolysin confers additional enzyme stability (12). Because IS*8* is located near the C terminus of the catalytic domain and resides within a surface loop (11), it could be involved in the interaction between the catalytic domain and the CTE, conferring additional enzyme stability.

Pyrolysin undergoes salt-induced autocleavage, and two of the cleavage sites are located within IS*29* and IS*27*. Disruption of ion pairs involving residues within and adjacent to IS*27* and IS*8* also leads to autocleavage of the enzyme at the same sites. These results clearly indicate that insert-mediated electrostatic interactions play important roles in maintaining pyrolysin structural integrity. Autocleavage is a well-known mechanism for irreversible inactivation of proteases, and the improvement of autoproteolytic stability is crucial for the application of proteases in biotechnology (28, 30). In rare cases, autocleavage products of proteases (e.g., chymotrypsin and WF146 protease) remain covalently linked through a disulfide bond to form active nicked enzymes (31, 32). Interestingly, pyrolysin autocleavage products form an enzymatically active nicked version of the protein despite lacking a disulfide bond. Although the nicked form is less stable and less active than intact pyrolysin, it has a half-life of approximately 6 h at 95°C and is stable enough to resist SDS and urea denaturation due to the intrinsically strong interactions between its structural elements. Obviously, the formation of a substantially stable and active nicked form contributes to the resistance of pyrolysin to irreversible inactivation due to autocleavage and thus prolongs its duration of action at high temperatures.

In our previous study, modifying the Ca2 site in the PPC domain of the CTE to eliminate unfavorable electrostatic repulsion (D818N/D820N) increased the thermostability of the enzyme (15). In this study, the R249E mutation within IS*29* improves enzyme thermostability and resistance to salt-induced autocleavage. This is likely due to removing unfavorable electrostatic interactions involving $Arg^{249}$. Moreover, when variants R249E and D818N/D820N are combined, the enzyme thermostability is improved further. The resulting variant R249E/D818N/D820N is both resistant to salt-induced autocleavage and exhibits a remarkably long half-life of approximately 36 h at 95°C. Improving thermostability by eliminating unfavorable electrostatic interactions has been reported previously for hyperthermostable CutA1 protein from *Pyrococcus horikoshii* (33). In addition, introduction of an ion pair network has been shown to improve the thermostability of glutamate dehydrogenases from *Thermococcus litoralis* (34) and *Thermococcus kodakarensis* KOD1 (35). Based on these results, electrostatic interaction optimization is an effective strategy to further stabilize hyperthermostable enzymes artificially.

## MATERIALS AND METHODS

**Materials.** Restriction enzymes and T4 DNA ligase were purchased from Fermentas (Burlington, Canada), DpnI was purchased from Thermo Scientific (Rockford, IL, USA), KOD-Plus-Neo DNA polymerase was from Toyobo (Osaka, Japan), azocasein and β-casein were from Sigma (St. Louis, MO, USA), and N-succinyl-Ala-Ala-Pro-Lys-*p*-nitroanilide (suc-AAPK-pNA) was from GL Biochem Ltd. (Shanghai, China).

**Bacterial strains and growth conditions.** *Escherichia coli* DH5α and BL21-CodonPlus (DE3)-RIL strains were used for cloning and expression, respectively. Bacteria were grown at 37°C in Luria-Bertani medium supplemented with kanamycin (30 μg/ml) and/or chloramphenicol (34 μg/ml) as needed.

**Plasmid construction and mutagenesis.** Expression plasmids used for the proforms of wild-type pyrolysin (Pls) (pET26b-*pls*) and the active-site variant PlsS441A (pET26-*plsS441A*) were constructed previously (12). Table S1 in the supplemental material lists the primer sequences used in this study. The genes encoding the proforms of the insert-deletion variants PlsΔIS*147*, PlsΔIS*29*, and PlsΔIS*27* were constructed using the megaprimer PCR method (36). The primer pairs are listed in Table S2. Briefly, the pET26b-*pls* template was combined with primer pls-F and specific mutagenic primers (plsΔIS*147*-R,

plsΔIS*29*-R, or plsΔIS*27*-R) for the first round of PCR to amplify the 5′ end of the coding sequence (megaprimers). Subsequently, genes encoding insert-deletion variant proforms were amplified from pET26b-*pls* using the megaprimers and primer pls-R. PCR products were digested with BamHI and XhoI and ligated into pET26b to generate the expression plasmids pET26b-*pls*ΔIS*147*, pET26b-*pls*ΔIS*29*, and pET26b-*pls*ΔIS*27*. The QuikChange site-directed mutagenesis (SDM) method (37) was used to construct the PlsΔIS*8* variant and the point mutants. Mutagenesis primer pairs are listed in Table S2. pET26b-*pls* underwent single or successive rounds of SDM to generate single and multiple mutation variants. The sequences of all recombinant plasmids were confirmed using DNA sequencing.

**Expression, activation, and purification.** Recombinant pyrolysin proform and its variants were produced in *E. coli* BL21-CodonPlus (DE3)-RIL as described previously (12). Cells were harvested, suspended in buffer A (20 mM HEPES, 10 mM NaOH, pH 7.5) containing 0.5 M NaCl, and sonicated on ice. After centrifugation at 13,000 × *g* for 10 min at 4°C, the insoluble fraction containing the recombinant proforms were retained and solubilized in buffer A containing 6 M urea. Samples were incubated at 4°C overnight and centrifuged at 13,000 × *g* for 10 min at 4°C. The resulting supernatants were dialyzed against buffer A at 4°C overnight to remove the urea and used as crude proform samples. To produce mature enzyme, the crude proform samples were incubated at 95°C for 2 h to activate the enzymes. The proforms and the mature forms were purified using a $Ni^{2+}$-charged chelating Sepharose Fast Flow column (GE Healthcare, Uppsala, Sweden) and a bacitracin-Sepharose 4B column (GE Healthcare), respectively, as described previously (15). The affinity purification procedure for the mature form of PlsΔIS*29* was similar to that of other mature variants (i.e., using a bacitracin-Sepharose 4B column), except 6 M urea was not included in the wash buffer. The enzyme solution was concentrated with a Microcon YM-3 centrifugal filter (Millipore, Bedford, MA, USA) as needed. The protein concentrations of the purified enzyme samples were measured using the Bradford method (38). The amount of target protein in crude samples was estimated from band intensities on SDS-PAGE gel with bovine serum albumin (BSA) as a standard.

**SDS-PAGE and gelatin overlay assay.** SDS-PAGE was performed using 12% polyacrylamide gel in the absence or presence of 8 M urea (urea–SDS-PAGE) in a Tris-glycine buffer system (39). In some cases, the Tris-tricine buffer (40) was used for tricine–SDS-PAGE analysis. Unless otherwise indicated, protein samples for SDS-PAGE were precipitated using TCA at a final concentration of 20% (wt/vol). Following incubation at room temperature for 15 min, precipitated proteins were recovered using centrifugation (13,000 × *g* for 10 min) and resuspended in ice-cold acetone. The proteins then were centrifuged at 13,000 × *g* for 10 min and air dried. Finally, the proteins were solubilized in loading buffer containing 8 M urea and electrophoresed without heating the sample. For protease activity staining, enzyme samples that had not been treated with TCA were mixed with loading buffer lacking 8 M urea and electrophoresed using SDS-PAGE or urea–SDS-PAGE. The gel overlay assay was then performed according to the method described by Blumentals et al. (5) with one revision: the proteolytic reaction was carried out at 90°C for 2 h in buffer A.

**Enzyme activity assay.** Unless otherwise indicated, the azocaseinolytic activity of the enzyme was assayed at 95°C for 30 min in 400 μl reaction mixture that contained 0.25% (wt/vol) azocasein and 200 μl of enzyme sample in buffer A (15). The reaction was terminated by the addition of 400 μl of 40% (wt/vol) TCA. After incubation at room temperature for 15 min, the mixture was centrifuged at 13,000 × *g* for 10 min, and the absorbance of the supernatant was measured at 335 nm in a 1-cm light-path cell. One unit of activity was defined as the amount of enzyme required to increase the $A_{335}$ value by 0.01 per min. For activity assays at temperatures above 100°C, the reaction was performed in screw-top tubes with O rings to prevent evaporation and a glycerol bath was used.

Using suc-AAPK-pNA as the substrate, kinetic parameters of the enzymes were determined at 90°C in buffer A. The activity was recorded by monitoring the initial velocity of suc-AAPK-pNA hydrolysis at 410 nm in a thermostated spectrophotometer (Cintra 10e; GBC, Australia). This velocity was calculated on the basis of an extinction coefficient for *p*-nitroaniline of 8,480 $M^{-1}$ $cm^{-1}$ at 410 nm. One unit of enzyme activity was defined as the amount of enzyme that produced 1 μmol pNA per min under the assay conditions. Kinetic parameters were calculated from the initial velocity of hydrolysis with a substrate concentration range of 0.1 to 15 mM (12). $K_m$ and $k_{cat}$ values were obtained using the nonlinear regression Table Curve 2D software (Jandel Scientific, version 5.0).

**Calcium ion content determination.** The buffers used in this experiment were prepared with ultrapure Milli-Q water. Glassware and plasticware were cleaned exhaustively with 97% ethanol, washed three times with double-distilled water, and then rinsed with Milli-Q water. The purified enzyme samples (100 to 150 μg/ml) were dialyzed at 4°C against buffer A three times. One milliliter of each sample was used for inductively coupled plasma mass spectrometry (ICP-MS; Agilent 7500ce) analysis. The calcium ion contents of dialysis buffers were also determined by ICP-MS and used as controls.

**N-terminal amino acid sequencing.** The proteins were separated by SDS-PAGE and electroblotted onto a polyvinylidene difluoride membrane. After staining with Coomassie brilliant blue R250, the target protein bands were excised and the N-terminal amino acids were sequenced using a PPSQ-33A protein sequencer (Shimadzu, Kyoto, Japan).

## SUPPLEMENTAL MATERIAL

Supplemental material for this article may be found at https://doi.org/10.1128/AEM.03228-16.

**TEXT S1**, PDF file, 0.62 MB.

## ACKNOWLEDGMENTS

We thank Bin Hu and Xiaoting Li (College of Chemistry and Molecular Sciences, Wuhan University, China) for their help with ICP-MS analysis.

This work was supported in part by the National Natural Science Foundation of China (31270099 and 31570062) and the National Infrastructure of Natural Resources for the Science and Technology Program of China (NIMR-2014-8).

We have no conflicts of interest to declare.

## REFERENCES

1. Stetter KO, Fiala G, Huber G, Huber R, Segerer A. 1990. Hyperthermophilic microorganisms. FEMS Microbiol Lett 75:117–124. https://doi.org/10.1111/j.1574-6968.1990.tb04089.x.
2. Vieille C, Zeikus GJ. 2001. Hyperthermophilic enzymes: sources, uses, and molecular mechanisms for thermostability. Microbiol Mol Biol Rev 65:1–43. https://doi.org/10.1128/MMBR.65.1.1-43.2001.
3. Atomi H, Sato T, Kanai T. 2011. Application of hyperthermophiles and their enzymes. Curr Opin Biotechnol 22:618–626. https://doi.org/10.1016/j.copbio.2011.06.010.
4. Fiala G, Stetter KO. 1986. *Pyrococcus furiosus* sp. nov. represents a novel genus of marine heterotrophic archaebacteria growing optimally at 100°C. Arch Microbiol 145:56–61. https://doi.org/10.1007/BF00413027.
5. Blumentals II, Robinson AS, Kelly RM. 1990. Characterization of sodium dodecyl sulfate-resistant proteolytic activity in the hyperthermophilic archaebacterium *Pyrococcus furiosus*. Appl Environ Microbiol 56:1992–1998.
6. Eggen R, Geerling A, Watts J, de Vos WM. 1990. Characterization of pyrolysin, a hyperthermoactive serine protease from the archaebacterium *Pyrococcus furiosus*. FEMS Microbiol Lett 71:17–20. https://doi.org/10.1111/j.1574-6968.1990.tb03791.x.
7. Connaris H, Cowan DA, Sharp RJ. 1991. Heterogeneity of proteinases from the hyperthermophilic archaeobacterium *Pyrococcus furiosus*. J Gen Microbiol 137:1193–1199. https://doi.org/10.1099/00221287-137-5-1193.
8. Snowden LJ, Blumentals II, Kelly RM. 1992. Regulation of proteolytic activity in the hyperthermophile *Pyrococcus furiosus*. Appl Environ Microbiol 58:1134–1141.
9. Voorhorst WGB, Eggen RIL, Geerling ACM, Platteeuw C, Siezen RJ, de Vos WM. 1996. Isolation and characterization of the hyperthermostable serine protease, pyrolysin, and its gene from the hyperthermophilic archaeon *Pyrococcus furiosus*. J Biol Chem 271:20426–20431. https://doi.org/10.1074/jbc.271.34.20426.
10. Siezen RJ, Leunissen JA. 1997. Subtilases: the superfamily of subtilisin-like serine proteases. Protein Sci 6:501–523.
11. Voorhorst WG, Warner A, de Vos WM, Siezen RJ. 1997. Homology modelling of two subtilisin-like proteases from the hyperthermophilic archaea *Pyrococcus furiosus* and *Thermococcus stetteri*. Protein Eng 10:905–914. https://doi.org/10.1093/protein/10.8.905.
12. Dai Z, Fu H, Zhang Y, Zeng J, Tang B, Tang XF. 2012. Insights into the maturation of hyperthermophilic pyrolysin and the roles of its N-terminal propeptide and long C-terminal extension. Appl Environ Microbiol 78:4233–4241. https://doi.org/10.1128/AEM.00548-12.
13. Mayr J, Lupas A, Kellermann J, Eckerskorn C, Baumeister W, Peters J. 1996. A hyperthermostable protease of the subtilisin family bound to the surface layer of the archaeon *Staphylothermus marinus*. Curr Biol 6:739–749. https://doi.org/10.1016/S0960-9822(09)00455-2.
14. Tomkinson B, Laoi BN, Wellington K. 2002. The insert within the catalytic domain of tripeptidyl-peptidase II is important for the formation of the active complex. Eur J Biochem 269:1438–1443. https://doi.org/10.1046/j.1432-1033.2002.02783.x.
15. Zeng J, Gao X, Dai Z, Tang B, Tang XF. 2014. Effects of metal ions on stability and activity of hyperthermophilic pyrolysin and further stabilization of this enzyme by modification of a $Ca^{2+}$-binding site. Appl Environ Microbiol 80:2763–2772. https://doi.org/10.1128/AEM.00006-14.
16. Rigden DJ, Galperin MY. 2004. The DxDxDG motif for calcium binding: multiple structural contexts and implications for evolution. J Mol Biol 343:971–984. https://doi.org/10.1016/j.jmb.2004.08.077.
17. Rigden DJ, Woodhead DD, Wong PW, Galperin MY. 2011. New structural and functional contexts of the Dx[DN]xDG linear motif: insights into evolution of calcium-binding proteins. PLoS One 6:e21507. https://doi.org/10.1371/journal.pone.0021507.
18. Daniel RM, Dines M, Petach HH. 1996. The denaturation and degradation of stable enzymes at high temperatures. Biochem J 317:1–11. https://doi.org/10.1042/bj3170001.
19. Takeuchi Y, Tanaka S, Matsumura H, Koga Y, Takano K, Kanaya S. 2009. Requirement of a unique $Ca^{2+}$-binding loop for folding of Tk-subtilisin from a hyperthermophilic archaeon. Biochemistry 48:10637–10643. https://doi.org/10.1021/bi901334b.
20. Jean L, Withers-Martinez C, Hackett F, Blackman MJ. 2005. Unique insertions within *Plasmodium falciparum* subtilisin-like protease-1 are crucial for enzyme maturation and activity. Mol Biochem Parasitol 144:187–197. https://doi.org/10.1016/j.molbiopara.2005.07.008.
21. Withers-Martinez C, Strath M, Hackett F, Haire LF, Howell SA, Walker PA, Christodoulou E, Dodson GG, Blackman MJ. 2014. The malaria parasite egress protease SUB1 is a calcium-dependent redox switch subtilisin. Nat Commun 5:3726.
22. Tanaka S, Saito K, Chon H, Matsumura H, Koga Y, Takano K, Kanaya S. 2007. Crystal structure of unautoprocessed precursor of subtilisin from a hyperthermophilic archaeon: evidence for $Ca^{2+}$-induced folding. J Biol Chem 282:8246–8255. https://doi.org/10.1074/jbc.M610137200.
23. Bryan P, Wang L, Hoskins J, Ruvinov S, Strausberg S, Alexander P, Almog O, Gilliland G, Gallagher T. 1995. Catalysis of a protein folding reaction: mechanistic implications of the 2.0 Å structure of the subtilisin-prodomain complex. Biochemistry 34:10310–10318. https://doi.org/10.1021/bi00032a026.
24. Schonegge AM, Villa E, Forster F, Hegerl R, Peters J, Baumeister W, Rockel B. 2012. The structure of human tripeptidyl peptidase II as determined by a hybrid approach. Structure 20:593–603. https://doi.org/10.1016/j.str.2012.01.025.
25. Rockel B, Kopec KO, Lupas AN, Baumeister W. 2012. Structure and function of tripeptidyl peptidase II, a giant cytosolic protease. Biochim Biophys Acta 1824:237–245. https://doi.org/10.1016/j.bbapap.2011.07.002.
26. Bryan P, Alexander P, Strausberg S, Schwarz F, Wang L, Gilliland G, Gallagher DT. 1992. Energetics of folding subtilisin BPN′. Biochemistry 31:4937–4945. https://doi.org/10.1021/bi00136a003.
27. Gros P, Kalk KH, Hol WG. 1991. Calcium binding to thermitase. Crystallographic studies of thermitase at 0, 5, and 100 mM calcium. J Biol Chem 266:2953–2961.
28. Bryan PN. 2000. Protein engineering of subtilisin. Biochim Biophys Acta 1543:203–222. https://doi.org/10.1016/S0167-4838(00)00235-1.
29. Xu BL, Dai M, Chen Y, Meng D, Wang Y, Fang N, Tang XF, Tang B. 2015. Improving the thermostability and activity of a thermophilic subtilase by incorporating structural elements of its psychrophilic counterpart. Appl Environ Microbiol 81:6302–6313. https://doi.org/10.1128/AEM.01478-15.
30. Fontana A, Fassina G, Vita C, Dalzoppo D, Zamai M, Zambonin M. 1986. Correlation between sites of limited proteolysis and segmental mobility in thermolysin. Biochemistry 25:1847–1851. https://doi.org/10.1021/bi00356a001.
31. Bódi Á, Kaslik G, Venekei I, Gráf L. 2001. Structural determinants of the half-life and cleavage site preference in the autolytic inactivation of chymotrypsin. Eur J Biochem 268:6238–6246. https://doi.org/10.1046/j.0014-2956.2001.02578.x.
32. Bian Y, Liang X, Fang N, Tang XF, Tang B, Shen P, Peng Z. 2006. The roles of surface loop insertions and disulfide bond in the stabilization of thermophilic WF146 protease. FEBS Lett 580:6007–6014. https://doi.org/10.1016/j.febslet.2006.09.068.
33. Matsuura Y, Takehira M, Sawano M, Ogasahara K, Tanaka T, Yamamoto H, Kunishima N, Katoh E, Yutani K. 2012. Role of charged residues in stabilization of *Pyrococcus horikoshii* CutA1, which has a denaturation temperature of nearly 150°C. FEBS J 279:78–90. https://doi.org/10.1111/j.1742-4658.2011.08400.x.

34. Vetriani C, Maeder DL, Tolliday N, Yip KSP, Stillman TJ, Britton KL, Rice DW, Klump HH, Robb FT. 1998. Protein thermostability above 100°C: a key role for ionic interactions. Proc Natl Acad Sci U S A 95:12300–12305. https://doi.org/10.1073/pnas.95.21.12300.
35. Rahman RN, Fujiwara S, Nakamura H, Takagi M, Imanaka T. 1998. Ion pairs involved in maintaining a thermostable structure of glutamate dehydrogenase from a hyperthermophilic archaeon. Biochem Biophys Res Commun 248:920–926. https://doi.org/10.1006/bbrc.1998.8933.
36. Sarkar G, Sommer SS. 1990. The "megaprimer" method of site-directed mutagenesis. Biotechniques 8:404–407.
37. Papworth C, Bauer JC, Braman J. 1996. Site-directed mutagenesis in one day with >80% efficiency. Strategies 9:3–4. https://doi.org/10.1080/08924562.1996.11000299.
38. Bradford MM. 1976. A rapid and sensitive method for the quantitation of microgram quantities of protein utilizing the principle of protein-dye binding. Anal Biochem 72:248–254. https://doi.org/10.1016/0003-2697(76)90527-3.
39. Laemmli UK. 1970. Cleavage of structural proteins during the assembly of the head of bacteriophage T4. Nature 227:680–685. https://doi.org/10.1038/227680a0.
40. Schagger H. 2006. Tricine-SDS-PAGE. Nat Protoc 1:16–22. https://doi.org/10.1038/nprot.2006.4.